

## Spin-torsion effects in the hyperfine structure of methanol

L. H. Coudert, C. Gutlé, T. R. Huet, J.-U. Grabow, and S. A. Levshakov

Citation: *The Journal of Chemical Physics* **143**, 044304 (2015); doi: 10.1063/1.4926942

View online: <http://dx.doi.org/10.1063/1.4926942>

View Table of Contents: <http://scitation.aip.org/content/aip/journal/jcp/143/4?ver=pdfcov>

Published by the [AIP Publishing](#)

---

### Articles you may be interested in

[The effects of methyl internal rotation and  \$^{14}\text{N}\$  quadrupole coupling in the microwave spectra of two conformers of  \$\text{N,N}\$ -diethylacetamide](#)

*J. Chem. Phys.* **141**, 204308 (2014); 10.1063/1.4901980

[Rotational spectroscopy of antipyretics: Conformation, structure, and internal dynamics of phenazone](#)

*J. Chem. Phys.* **138**, 114304 (2013); 10.1063/1.4794693

[Nuclear electric quadrupole moments of Rb from the hyperfine spectrum of  \$\text{RbF}\$](#)

*J. Chem. Phys.* **124**, 244304 (2006); 10.1063/1.2212414

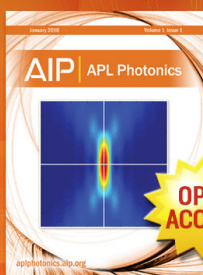
[Hyperfine structure and the Stark effect in the electronic spectrum of the  \$\text{SiCH}\$  radical with implications for microwave spectroscopy and radioastronomy](#)

*J. Chem. Phys.* **115**, 817 (2001); 10.1063/1.1378818

[Perturbation-allowed rotational transitions and  \$A\_1 - A\_2\$  splitting transitions in the ground,  \$v\_2 = 1\$  and  \$v\_4 = 1\$  vibrational states of  \$\text{SbH}\_3\$  observed by microwave Fourier transform spectroscopy: Extension of the effective hyperfine Hamiltonian](#)

*J. Chem. Phys.* **114**, 3508 (2001); 10.1063/1.1342013

---



Launching in 2016!  
The future of applied photonics research is here

OPEN  
ACCESS

**AIP** | APL  
Photonics

## Spin-torsion effects in the hyperfine structure of methanol

L. H. Coudert,<sup>1,a)</sup> C. Gutlé,<sup>1</sup> T. R. Huet,<sup>2</sup> J.-U. Grabow,<sup>3</sup> and S. A. Levshakov<sup>4,b)</sup>

<sup>1</sup>Laboratoire Inter-Universitaire des Systèmes Atmosphériques, UMR 7583 CNRS-Universités Paris Est Créteil et Paris Diderot, 61 Avenue du Général de Gaulle, 94010 Créteil Cedex, France

<sup>2</sup>Laboratoire de Physique des Lasers, Atomes et Molécules, UMR 8523 CNRS-Université Lille 1, Bâtiment P5, 59655 Villeneuve d'Ascq Cedex, France

<sup>3</sup>Institut für Physikalische Chemie, Callinstrasse 3–3a, 30167 Hannover, Germany

<sup>4</sup>St. Petersburg Electrotechnical University “LETI,” 197376 St. Petersburg, Russia

(Received 2 April 2015; accepted 6 July 2015; published online 23 July 2015)

The magnetic hyperfine structure of the non-rigid methanol molecule is investigated experimentally and theoretically. 12 hyperfine patterns are recorded using molecular beam microwave spectrometers. These patterns, along with previously recorded ones, are analyzed in an attempt to evidence the effects of the magnetic spin-torsion coupling due to the large amplitude internal rotation of the methyl group [J. E. M. Heuvel and A. Dymanus, *J. Mol. Spectrosc.* **47**, 363 (1973)]. The theoretical approach setup to analyze the observed data accounts for this spin-torsion in addition to the familiar magnetic spin-rotation and spin-spin interactions. The theoretical approach relies on symmetry considerations to build a hyperfine coupling Hamiltonian and spin-rotation-torsion wavefunctions compatible with the Pauli exclusion principle. Although all experimental hyperfine patterns are not fully resolved, the line position analysis yields values for several parameters including one describing the spin-torsion coupling. © 2015 AIP Publishing LLC. [<http://dx.doi.org/10.1063/1.4926942>]

### I. INTRODUCTION

Molecular hyperfine effects in which hyperfine coupling arises from equivalent nuclei that can be exchanged by either rotations or large amplitude motions are of great interest and lead to unexpected results. In  $C_{3v}$  symmetry rigid molecules like chloroform and trichlorofluoromethane, the three chlorine atoms giving rise to the hyperfine quadrupole coupling can be exchanged by  $2\pi/3$  rotations about the  $C_3$  axis of symmetry leading to an effective hyperfine coupling Hamiltonian depending qualitatively on the  $A$  or  $E$  nature of the rotational levels.<sup>1</sup> Similar effects are observed in non-rigid molecules. In hydrazine, the coupling between the large amplitude motions and the hyperfine quadrupole coupling arising from the two nitrogen atoms leads to hyperfine patterns in which these two atoms are either equivalent or not, depending on the symmetry species of the tunneling levels.<sup>2</sup> These effects are even more striking in deuterated acetylene dimer  $(C_2D_2)_2$  and deuterated water dimer  $(D_2O)_2$  in which the hyperfine structure arising for nondegenerate tunneling sublevels can be accounted for using an effective quadrupole coupling Hamiltonian with the same coupling constant for all four deuterium atoms.<sup>3,4</sup> In the non-rigid triply deuterated isotopic species of acetaldehyde  $CD_3COH$ , the three equivalent deuterium atoms are exchanged by the large amplitude torsional motion leading to hyperfine patterns which are also qualitatively dependent on the torsional symmetry of the levels.<sup>5</sup>

This paper is devoted to experimental and theoretical analyses of the hyperfine structure of the normal species

of methanol which is of great relevance for high-precision astrophysics and theoretical physics.<sup>6</sup> The hyperfine structure of several transitions was recorded in the microwave domain and analyzed with a view towards understanding the effects of the large amplitude torsional motion. The hyperfine coupling in methanol is due to the well known magnetic spin-rotation and spin-spin couplings<sup>7,8</sup> leading to small line splittings on the order of 10 kHz. Due to the large amplitude internal rotation of the methyl group, averaging effects similar to those described above are expected as the large amplitude motion exchanges three equivalent hydrogen atoms. The large amplitude internal rotation may also lead to a less known magnetic coupling, the so-called spin-torsion coupling, which was first studied by Heuvel and Dymanus<sup>9,10</sup> and later by Hougen *et al.*<sup>11</sup> and which has not yet been conclusively evidenced.

The theoretical approach used in the present paper relies on careful symmetry considerations and is based on an effective hyperfine Hamiltonian expressed with the help of symmetrized coupling operators<sup>12</sup> describing the spin-rotation, spin-spin, and spin-torsion magnetic couplings. The constants involved in the operators corresponding to the spin-rotation and spin-spin interactions are evaluated using either *ab initio* calculations or the structure of the molecule. A tentative determination of the constants involved in the operators corresponding to spin-torsion is also performed based only on the structure of the molecule and ignoring electronic effects.

In the analysis of the hyperfine patterns, rotation-torsion matrix elements arising in the effective hyperfine Hamiltonian are computed for the rotation-torsion levels involved in the experimental data set, their rotation-torsion wavefunction being retrieved from the high-resolution spectroscopic data available for methanol (see, for instance, Xu *et al.*<sup>13</sup> and references therein). The line frequency analysis allows us to refine

<sup>a)</sup>Electronic mail: laurent.coudert@lisa.u-pec.fr

<sup>b)</sup>Permanent address: Ioffe Physical-Technical Institute, Politekhnicheskaya 26, 194021 St. Petersburg, Russia.

the constants involved in the operators describing the spin-rotation coupling and to carry out the first determination of the constants involved in the operators describing the spin-torsion coupling.

In the paper, the microwave measurements are described in Section II and the theoretical approach used to account for the magnetic hyperfine energy is introduced in Section III. In Section IV, the fitting hyperfine Hamiltonian is derived and the constants involved in this operator are numerically evaluated. Section V deals with the analysis of the hyperfine patterns. A discussion is given in Section VI.

## II. EXPERIMENTAL DATA

Three data sets were considered in the analysis. The first one was recorded using the Fourier transform microwave (FT-MW) spectrometer<sup>14,15</sup> in Hannover covering the range 2–26.5 GHz and described previously.<sup>16</sup> The molecular beam was generated as a pulsed supersonic expansion of a CH<sub>3</sub>OH/Ne mixture at a total backing pressure of 2 bars using a 1 mm-diameter nozzle orifice. Molecular pulses of approximately 0.25 ms duration were found optimal. The molecular response after MW impulse excitation was recorded in the time-domain; its signal frequencies were determined by Fourier transformation. The pulsed supersonic jet, exhibiting rotational temperatures of 2 K, was introduced coaxially to the axis of the Fabry-Perot resonator, and consequently, each observed transition appears as a Doppler doublet. The line center is determined as the arithmetic mean of the peak frequencies of the two Doppler components. The accuracy of spectral line positions is estimated to be better than 2 kHz. All frequency measurements were referenced to a global position system (GPS) controlled frequency standard (relative frequency accuracy: 10<sup>-11</sup>). Figure 1 shows the spectrum recorded for the

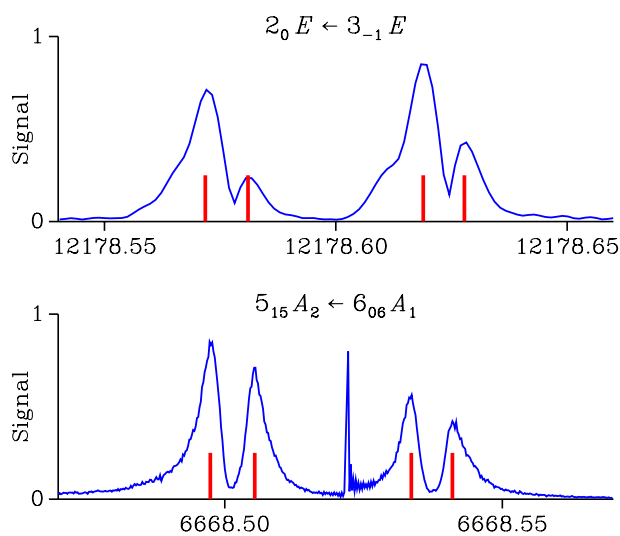


FIG. 1. Upper and lower panels show the spectrum of the  $2_0 E \leftarrow 3_{-1} E$  and  $5_{15} A_2 \leftarrow 6_{06} A_1$  rotation-torsion transitions recorded using the experimental setup in Hannover and Lille, respectively. Both setups give rise to hyperfine lines split into two Doppler components. The Doppler splittings are 23 and 18 kHz for the spectra in the upper and lower panels, respectively. Both rotation-torsion transitions display a doublet structure. Solid vertical lines indicate the frequency of the observed lines. In the spectrum recorded with the experimental setup in Lille, the feature near 6668.525 MHz is an artefact.

hyperfine pattern of the transition at 12 178 MHz involving doubly degenerate  $E$ -type torsional levels. When accurate frequency measurements as those presented in this paper are carried out, the effects of the residual magnetic field in the spectrometer should be taken into account. Its value was estimated to be in the 0.5–1 G range. In a closed-shell molecule like methanol, such a residual magnetic field should not lead to noticeable effects.

The second set of data was recorded using the molecular beam FT-MW spectrometer in Lille. In this spectrometer, mirrors with a diameter of 0.7 m are used<sup>17,18</sup> allowing us to record signals in the 2–20 GHz spectral region. The sample was purchased at Sigma Aldrich (Fluka Chemie GmbH), with a purity of 99.8%, and used without further purification. Methanol vapors at a pressure of 30 mbars were mixed with neon carrier gas at a backing pressure of 1.6 bars. The mixture was introduced into the Fabry-Perot cavity at a repetition rate of 1.5 Hz. Molecules were polarized within the supersonic expansion by a 2  $\mu$ s pulse and the free induction decay signal was detected and digitized at a sampling rate of 120 MHz. After transformation from the time domain signal into the frequency domain, molecular lines were observed as Doppler doublets, with a signal point every 0.46 kHz. Each average spectrum was obtained by co-adding about 100 signals. Transition frequencies were measured as the mean value of the two Doppler components and for most lines the uncertainty of the measurements is estimated to be less than 1 kHz. The Doppler width is a few kHz. No attempts were made to obtain transition frequencies from the time domain signal. Figure 1 displays the hyperfine structure recorded with the experimental setup in Lille of a transition involving nondegenerate  $A$ -type torsional levels.

The third set of data comes from the experimental investigation of Heuvel and Dymanus.<sup>9</sup> The frequencies measured by these authors are reported in their Table I except for the  $1_{01} A_2 \leftarrow 0_{00} A_1$  transition. For this transition, the measured frequencies of the hyperfine components were retrieved from their Fig. 2 using a graphical approach. The following six frequencies were obtained: 48 372.437 25, 48 372.440 69, 48 372.448 50, 48 372.452 25, 48 372.466 25, and 48 372.477 87 MHz with relative intensities close to the theoretical ones: 1/3, 1, 5/3, 7/3, 5/3, and 1, respectively.

Plots of the 19 experimental hyperfine patterns described above as well as their hyperfine frequencies are given in a figure available in the supplementary material.<sup>19</sup> For hyperfine patterns measured with different experimental setups, there is a good consistency and the frequencies of the hyperfine components agree within 0.7 kHz for rotation-torsion transitions involving  $A$ -type levels. For transitions involving  $E$ -type levels, the agreement is usually less satisfactory. In the case of the  $2_0 E \leftarrow 3_{-1} E$  transition at 12 178 MHz, measured with the Lille and Hannover experimental setups, the hyperfine pattern is barely resolved with the former setup while it is well resolved with the latter. In addition to a 5 kHz discrepancy for the frequency of the higher lying hyperfine component, the intensities of the hyperfine components do not match. In the case of the  $9_{-1} E \leftarrow 8_{-2} E$  transitions at 9936 MHz, the pattern recorded with the Hannover experimental setup displays 5 lines while the one recorded with the Lille exper-

TABLE I. Available measurements.

Transition <sup>a</sup>	Frequency <sup>b</sup>	Experimental setup <sup>c</sup>	Nature <sup>d</sup>
$2_{11} A_2 \leftarrow 2_{12} A_1$	2 502.8	Reference <sup>9e</sup> and Lille	S
$3_{12} A_1 \leftarrow 3_{13} A_2$	5 005.3	Reference <sup>9e</sup> and Lille	D
$5_{15} A_2 \leftarrow 6_{06} A_1$	6 668.5	Hannover and Lille <sup>e</sup>	D
$9_{-1} E \leftarrow 8_{-2} E$	9 936.2	Hannover and Lille	
$4_{32} A_1 \leftarrow 5_{23} A_2$	9 978.7	Lille	
$2_0 E \leftarrow 3_{-1} E$	12 178.6	Hannover <sup>e</sup> and Lille	D
$6_{15} A_2 \leftarrow 6_{16} A_1$	17 513.3	Reference <sup>9e</sup>	D
$2_1 E \leftarrow 3_0 E$	19 967.4	Hannover <sup>e</sup>	S
$3_2 E \leftarrow 3_1 E$	24 928.7	Hannover <sup>e</sup>	D
$4_2 E \leftarrow 4_1 E$	24 933.5	Hannover <sup>e</sup>	D
$2_2 E \leftarrow 2_1 E$	24 934.4	Hannover <sup>e</sup>	S
$5_2 E \leftarrow 5_1 E$	24 959.1	Hannover <sup>e</sup>	D
$6_2 E \leftarrow 6_1 E$	25 018.1	Hannover <sup>e</sup>	D
$1_{01} A_2 \leftarrow 0_{00} A_1$	48 372.4	Reference <sup>9e</sup>	M

<sup>a</sup>The assignment of the rotation-torsion transition for which hyperfine data are available is given in this column. All transitions are within the ground  $v_t = 0$  torsional level.

<sup>b</sup>Transition frequencies are given in this column in MHz.

<sup>c</sup>The experimental setup used to record the hyperfine structure or the reference from which hyperfine frequencies were taken are listed in this column.

<sup>d</sup>The nature of the observed hyperfine pattern. S, D, and M stand for singlet, doublet, and multiplet, respectively. A blank entry means that the nature of the hyperfine pattern could not be determined.

<sup>e</sup>Transition included in the analysis reported in Section V. Experimental frequencies measured with this setup were taken.

imental setup is not resolved. The measurement discrepancies for these two patterns may originate from the different durations of the polarizing pulse.

Table I lists the rotation-torsion transitions considered in this work as well as the experimental setup, or the reference, from which hyperfine frequencies were taken. The transitions fitted in the analysis reported in Section V are indicated along with the nature of the observed hyperfine pattern. In most cases, a doublet structure was observed; in three cases, a singlet structure; and, in the case of the  $1_{01} A_2 \leftarrow 0_{00} A_1$  transition, a multiplet structure. The  $9_{-1} E \leftarrow 8_{-2} E$  transition was not considered in the analysis as the exact nature of the observed hyperfine pattern could not be determined due to measure-

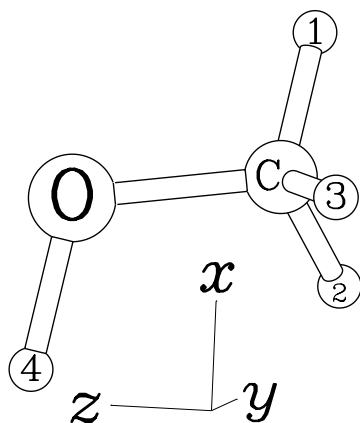


FIG. 2. The atom numbering chosen in this work is shown. The three hydrogen atoms of the methyl group are numbered 1, 2, and 3; the hydrogen atom of the hydroxyl group is atom 4. The molecule-fixed  $xyz$  axis system can also be seen. For clarity, its origin was not drawn at the molecular center of mass. The configuration shown corresponds to a value of the torsional angle  $\alpha$  of  $10^\circ$ . When  $\alpha = 0$ , hydrogen atom 1 lies in the  $xz$  plane.

ment inconsistencies. The  $4_{32} A_1 \leftarrow 5_{23} A_2$  transition was not considered either. Its observed hyperfine pattern did not match the calculated one displaying a complicated multiplet structure with close lying lines which may not have been resolved by the spectrometer.<sup>19</sup>

### III. THEORY

The theoretical approach developed in the present paper closely parallels those setups in the case of the non-rigid  $\text{CD}_3\text{COH}$  and  $\text{HCOOCH}_3$  molecules by Coudert and Lopez<sup>5</sup> and Tudorie *et al.*,<sup>12</sup> respectively. The coordinate system, the symmetry group, and the rotation-torsion Hamiltonian, briefly described in this section, are the same as those adopted in these references. Below, the magnetic hyperfine coupling Hamiltonian, including spin-torsion effects,<sup>10</sup> is expressed in terms of symmetry adapted rotation-torsion and hyperfine coupling operators. Hyperfine matrix elements for the hyperfine Hamiltonian are written with the help of several hyperfine coupling constants.

#### A. Coordinate system and rotation-torsion Hamiltonian

The coordinates<sup>5,12</sup> used in this work consist of the three usual Euler angles and of the large amplitude coordinate  $\alpha$  corresponding to the torsional angle of the methyl group with respect to the frame containing the oxygen and carbon atoms and the hydrogen atom of the hydroxyl group. The molecule-fixed  $xyz$  axis system is attached to the molecule so that its origin is at the molecule center of mass. The three atoms of the frame and the axis of internal rotation are held fixed in this axis system and lie in the  $xz$  plane. The position of the atoms of the molecule as well as the molecule-fixed axis system is illustrated in Fig. 2. This figure emphasizes that the three equivalent hydrogen atoms of the methyl group are numbered 1, 2, and 3; the hydrogen atom of the hydroxyl group being atom number 4. When  $\alpha = 0$ , hydrogen atom 1 lies in the  $xz$  plane and is *anti* to hydrogen atom 4. As stressed by Hougen *et al.*,<sup>20</sup> the symmetry group to be used is  $G_6$ ; its character table and the transformation properties of the coordinates are given in Tables VII and VIII of this reference.

The Hamiltonian used to calculate rotation-torsion energy levels is the rho axis method (RAM) internal-rotation Hamiltonian based on the work of Kirtman,<sup>21</sup> Lees and Baker,<sup>22</sup> and Herbst *et al.*<sup>23</sup> and reviewed by Hougen *et al.*<sup>20</sup> The RAM Hamiltonian, given in Eq. (26) of this reference, displays only one rotation-torsion Coriolis coupling term,

$$-2\rho F p_\alpha J_z, \quad (1)$$

where  $p_\alpha$  is the momentum conjugated to  $\alpha$ ;  $J_z$  is the  $z$ -component of the rotational angular momentum in the molecule-fixed axis system; and  $\rho$  and  $F$  are two constants depending on the geometry of the molecule.<sup>20</sup> The rotation-torsion terms needed to account for distortion effects are listed in Table 2 of Xu *et al.*<sup>13</sup> For a given rotation-torsion level characterized by the rotational quantum numbers  $JK_a K_c$ , by its symmetry species  $\Gamma$  in  $G_6$ , and by the torsional quantum number  $v_t$ , the rotation-torsion wavefunction will be written  $\Psi_{JK_a K_c, v_t}^\Gamma$

and expanded using the basis set functions in Eqs. (4)–(6) of Coudert and Lopez.<sup>5</sup> For the  $E_a$  and  $E_b$  component functions of a doubly degenerate level, the standard transformation properties given in the end of Section 3.2 of this reference will be used.

## B. Symmetry adapted hyperfine coupling operators and wavefunctions

The magnetic hyperfine coupling Hamiltonian  $H_{\text{hfs}}$  to be used for methanol is given in Eq. (26) of Heuvel and Dymanus<sup>10</sup> and contains three terms corresponding to the spin-rotation, spin-torsion, and spin-spin couplings. The former and latter couplings are not modified by the internal rotation and have the same form<sup>7,8</sup> as in a rigid molecule. In this investigation, all three interactions will be described using operators appropriate for  $\Delta J = 0$  matrix elements.<sup>11,12,24,25</sup> The operator for the spin-rotation coupling will be denoted  $H_{sr}$  and should be obtained by adding the contribution of all hydrogen atoms,

$$H_{sr} = \sum_{i=1}^4 H_{sr}^i = \sum_{i=1}^4 (\mathbf{I}_i \cdot \mathbf{J}) E^i, \quad (2)$$

where  $H_{sr}^i$  is the operator defined in Eq. (2) of Coudert *et al.*<sup>25</sup> describing the spin-rotation coupling for hydrogen atom  $i$ ;  $E^i$  is the  $\alpha$ -dependent rotation-torsion operator defined in Eq. (4) of the same reference;  $\mathbf{I}_i$  is the nuclear spin angular momentum; and  $\mathbf{J}$  is the rotational angular momentum. Similarly, the operator used for the spin-spin coupling  $H_{ss}$  is built by adding the contribution of the six pairs of hydrogen atoms,

$$H_{ss} = \sum_{i < j}^4 H_{ss}^{ij} = \sum_{i < j}^4 F(\mathbf{I}_i, \mathbf{I}_j, \mathbf{J}) S^{ij}, \quad (3)$$

where  $H_{ss}^{ij}$  is the operator defined in Eq. (6) of Coudert *et al.*<sup>25</sup> describing the spin-spin coupling between hydrogen atoms  $i$  and  $j$ ;  $F(\mathbf{I}_i, \mathbf{I}_j, \mathbf{J})$  is the hyperfine operator introduced in Eq. (7) of the same reference; and  $S^{ij}$  is the  $\alpha$ -dependent rotation-torsion operator defined for Eqs. (16) of Coudert *et al.*<sup>25</sup> The operator for the spin-torsion coupling  $H_{st}$ , deduced from Eq. (26) of Heuvel and Dymanus,<sup>10</sup> is given below using the form convenient for  $\Delta J = 0$  matrix elements<sup>11</sup> and adding the contribution of all hydrogen atoms,

$$H_{st} = \sum_{i=1}^4 H_{st}^i = \sum_{i=1}^4 (\mathbf{I}_i \cdot \mathbf{J}) G^i, \quad (4)$$

where  $G^i$  is an  $\alpha$ -dependent rovibrational operator. Using Eq. (10a) of Heuvel and Dymanus<sup>10</sup> and remembering that the RAM is used, this rovibrational operator can be expressed as

$$G^i = \{\rho J_z + p_\alpha, \sum_{\beta} J_{\beta} d_{\beta}^i\} / [2J(J+1)], \quad (5)$$

where  $\{, \}$  is the anticommutator;  $\beta$  runs over molecule-fixed coordinates  $x, y, z$ ;  $J_{\beta}$  are the components of the rotational angular momentum in the molecule-fixed axis system;  $d_{\beta}^i$  are the  $\alpha$ -dependent components in this axis system of the vector introduced by Heuvel and Dymanus;<sup>10</sup> and  $p_{\alpha}$  and  $\rho$  are defined as for Eq. (1).

As in Tudorie *et al.*,<sup>12</sup> the spin-rotation, spin-spin, and spin-torsion coupling operators in Eqs. (2)–(4) are rewritten in terms of products of symmetry-adapted hyperfine and rovibrational operators, characterized by their symmetry species in  $G_6$ . As hyperfine operators involve laboratory-fixed components of various angular momenta, they can only have  $A_1$ ,  $E_a$ , or  $E_b$  symmetry. The rovibrational operators will also belong to one of these three symmetry species so as to ensure a completely symmetrical hyperfine coupling Hamiltonian. The following expansion is found for the spin-rotation coupling:

$$H_{sr} = H_{sr}(A_1) \cdot O_{sr}(A_1) + H_{sr}^h(A_1) \cdot O_{sr}^h(A_1) + H_{sr}(E_a) \cdot O_{sr}(E_a) + H_{sr}(E_b) \cdot O_{sr}(E_b), \quad (6)$$

where a superscripted  $h$  indicates operator involving a contribution from the hydroxyl group hydrogen atom. In this equation, the hyperfine and rovibrational operators  $H_{sr}(\Gamma)$  and  $O_{sr}(\Gamma)$ , with  $\Gamma = A_1, E_a$ , and  $E_b$ , should be obtained from Eqs. (4) and (5) of Tudorie *et al.*,<sup>12</sup> respectively. The hyperfine and rovibrational operators  $H_{sr}^h(A_1)$  and  $O_{sr}^h(A_1)$  are the following:

$$H_{sr}^h(A_1) = \mathbf{I}_4 \cdot \mathbf{J} \quad \text{and} \quad O_{sr}^h(A_1) = E^4. \quad (7)$$

In the case of the spin-spin coupling, the expansion in terms of symmetry adapted operators contains twice as much terms than when the contribution from the hydroxyl group hydrogen atom is ignored,<sup>12</sup>

$$H_{ss} = H_{ss}(A_1) \cdot O_{ss}(A_1) + H_{ss}^h(A_1) \cdot O_{ss}^h(A_1) + H_{ss}(E_a) \cdot O_{ss}(E_a) + H_{ss}(E_b) \cdot O_{ss}(E_b) + H_{ss}^h(E_a) \cdot O_{ss}^h(E_a) + H_{ss}^h(E_b) \cdot O_{ss}^h(E_b), \quad (8)$$

where the superscripted  $h$  has the same meaning as for Eq. (6). In Eq. (8), the hyperfine and rovibrational operators  $H_{ss}(\Gamma)$  and  $O_{ss}(\Gamma)$ , with  $\Gamma = A_1, E_a$ , and  $E_b$ , should be obtained from Eqs. (6) and (7) of Tudorie *et al.*,<sup>12</sup> respectively. The hyperfine operators  $H_{ss}^h(\Gamma)$ , with  $\Gamma = A_1, E_a$ , and  $E_b$ , are the following:

$$\begin{cases} H_{ss}^h(A_1) = F_{14} + F_{24} + F_{34}, \\ H_{ss}^h(E_a) = \frac{1}{2}(2F_{14} - F_{24} - F_{34}), \\ H_{ss}^h(E_b) = \frac{\sqrt{3}}{2}(F_{24} - F_{34}), \end{cases} \quad (9)$$

where  $F_{ij}$  is a shorthand notation for  $F(\mathbf{I}_i, \mathbf{I}_j, \mathbf{J})$ . The rotation-torsion operators  $O_{ss}^h(\Gamma)$ , with  $\Gamma = A_1, E_a$ , and  $E_b$ , take the following expression:

$$\begin{cases} O_{ss}^h(A_1) = \frac{1}{3}(S^{14} + S^{24} + S^{34}), \\ O_{ss}^h(E_a) = \frac{1}{3}(2S^{14} - S^{24} - S^{34}), \\ O_{ss}^h(E_b) = \frac{1}{\sqrt{3}}(S^{24} - S^{34}). \end{cases} \quad (10)$$

The expansion in terms of symmetry adapted operators for the spin-torsion coupling is the following:

$$H_{st} = H_{st}(A_1) \cdot O_{st}(A_1) + H_{st}^h(A_1) \cdot O_{st}^h(A_1) + H_{st}(E_a) \cdot O_{st}(E_a) + H_{st}(E_b) \cdot O_{st}(E_b). \quad (11)$$

The hyperfine operators in this equation are the same as for the spin-rotation coupling in Eqs. (6) and (7). The rovibrational

operators are, however, different. Operators  $O_{st}^h(A_1)$  and  $O_{sr}(\Gamma)$ , with  $\Gamma = A_1, E_a$ , and  $E_b$ , should be obtained from Eq. (7) of the present paper and Eq. (5) of Tudorie *et al.*<sup>12</sup> after changing the rotation-torsion operators  $E^i$  into  $G^i$ .

The nuclear spin wavefunction is written in the coupled basis set  $|(I_1, I_{23})I_{123}, I_4, I\rangle$  corresponding to the coupling scheme,

$$\begin{aligned} \mathbf{I}_2 + \mathbf{I}_3 &= \mathbf{I}_{23}, \\ \mathbf{I}_1 + \mathbf{I}_{23} &= \mathbf{I}_{123}, \\ \mathbf{I}_{123} + \mathbf{I}_4 &= \mathbf{I}. \end{aligned} \quad (12)$$

In agreement with Bersohn<sup>26</sup> and using the same ideas as in the subsequent investigations of Swidzinski,<sup>27</sup> Wolf *et al.*,<sup>1</sup> and Bhattacharjee *et al.*,<sup>3</sup> about the hyperfine coupling in molecules with equivalent nuclei, symmetry adapted nuclear spin wavefunctions  $|\mu, I\rangle$  are built and are characterized by their symmetry species  $\mu$  in  $S_3$ , the permutation group of 3 particles, and by  $I$  the value of the total nuclear spin angular momentum. These wavefunctions are expressed in terms of nuclear spin wavefunctions as

$$\begin{cases} |A_1, 2\rangle = |(I_1, I_{23} = 1)I_{123} = 3/2, I_4, I = 2\rangle, \\ |A_1, 1\rangle = |(I_1, I_{23} = 1)I_{123} = 3/2, I_4, I = 1\rangle, \\ |E_a, 1\rangle = |(I_1, I_{23} = 1)I_{123} = 1/2, I_4, I = 1\rangle, \\ |E_a, 0\rangle = |(I_1, I_{23} = 1)I_{123} = 1/2, I_4, I = 0\rangle, \\ |E_b, 1\rangle = |(I_1, I_{23} = 0)I_{123} = 1/2, I_4, I = 1\rangle, \\ |E_b, 0\rangle = |(I_1, I_{23} = 0)I_{123} = 1/2, I_4, I = 0\rangle, \end{cases} \quad (13)$$

with the help of projection operators and using the fact<sup>1,3,26,27</sup> that the effects of a symmetry permutation of two nuclei on a nuclear spin wavefunction written in the coupled basis set can be evaluated with 6-j or 9-j symbols. In Eqs. (13),  $S_3$  being isomorphic to  $G_6$ , the symmetry species labels of the latter group are used. For doubly degenerate symmetry species, component functions obey the standard transformation properties chosen in the end of Section III A.

### C. Hyperfine energy levels

Matrix elements of the hyperfine Hamiltonian  $H_{\text{hfs}}$  are evaluated using the rotation-torsion-nuclear spin wavefunctions given in Eq. (10) of Tudorie *et al.*<sup>12</sup> where the symmetry adapted nuclear spin wavefunctions should be replaced by those in Eqs. (13). The following matrix element arises:

$$\langle n', \mu', I', F | H_{\text{hfs}} | n, \mu, I, F \rangle, \quad (14)$$

where  $n'$  and  $n$  are shorthand notations for the quantum numbers of a rotation-torsion level.<sup>12</sup> Using the results in Sec. III B, the above matrix element is expressed as

$$\sum_i C_i \times \langle J', \mu', I', F | H_i | J, \mu, I, F \rangle, \quad (15)$$

where  $C_i$  is a hyperfine coupling constant equal to the rotation-torsion matrix element  $\langle n' | O_i | n \rangle$  of the symmetry adapted rotation-torsion operator  $O_i$  and the hyperfine matrix element is that of the symmetry adapted hyperfine operator  $H_i$ . In the case of a nondegenerate level,  $n' = n$  and Eq. (14) leads to the coupling constants and hyperfine matrix elements listed in

TABLE II. Hyperfine coupling constants, rotation-torsion matrix elements, and hyperfine matrix elements to be used for nondegenerate rotation-torsion levels.

Coupling constant	Rotation-torsion matrix element <sup>a</sup>	Hyperfine matrix element <sup>b</sup>
$C_S^{sr}$	$\langle n   O_{sr}(A_1)   n \rangle$	$\langle m'   H_{sr}(A_1)   m \rangle$
$C_S^{sr,h}$	$\langle n   O_{sr}^h(A_1)   n \rangle$	$\langle m'   H_{sr}^h(A_1)   m \rangle$
$C_S^{ss}$	$\langle n   O_{ss}(A_1)   n \rangle$	$\langle m'   H_{ss}(A_1)   m \rangle$
$C_S^{ss,h}$	$\langle n   O_{ss}^h(A_1)   n \rangle$	$\langle m'   H_{ss}^h(A_1)   m \rangle$
$C_S^{st}$	$\langle n   O_{st}(A_1)   n \rangle$	$\langle m'   H_{st}(A_1)   m \rangle$
$C_S^{st,h}$	$\langle n   O_{st}^h(A_1)   n \rangle$	$\langle m'   H_{st}^h(A_1)   m \rangle$

<sup>a</sup>The hyperfine coupling constant is equal to the matrix element of a rotation-torsion operator within the wavefunction of a nondegenerate rotation-torsion level labeled with the shorthand notation  $n$ .

<sup>b</sup>The hyperfine matrix element that factors the hyperfine coupling constant is given in this column.  $|m\rangle$  and  $|m'\rangle$  are shorthand notations for  $|J, A_1, I, F\rangle$  and  $|J, A_1, I', F\rangle$ , respectively.

Table II. We can see that although there are six hyperfine coupling constants only four different hyperfine operators arise. In the case of a doubly degenerate rotation-torsion level, Eq. (14) should be evaluated within as well between the

TABLE III. Hyperfine coupling constants, rotation-torsion matrix elements, and hyperfine matrix elements to be used for doubly degenerate rotation-torsion levels.

Coupling constant <sup>a</sup>	Rotation-torsion matrix element <sup>b</sup>	Hyperfine matrix element <sup>c</sup>
$C_S^{sr}$	$\langle n_a   O_{sr}(A_1)   n_a \rangle$	$\langle m'   H_{sr}(A_1)   m \rangle$
...	$\langle n_b   O_{sr}(A_1)   n_b \rangle$	$\langle m'   H_{sr}(A_1)   m \rangle$
$C_A^{sr}$	$\langle n_a   O_{sr}(E_a)   n_a \rangle$	$\langle m'   H_{sr}(E_a)   m \rangle$
...	$-\langle n_b   O_{sr}(E_a)   n_b \rangle$	$\langle m'   H_{sr}(E_a)   m \rangle$
...	$-\langle n_a   O_{sr}(E_b)   n_b \rangle$	$\langle m'   H_{sr}(E_b)   m \rangle$
$C_S^{sr,h}$	$\langle n_a   O_{sr}^h(A_1)   n_a \rangle$	$\langle m'   H_{sr}^h(A_1)   m \rangle$
...	$\langle n_b   O_{sr}^h(A_1)   n_b \rangle$	$\langle m'   H_{sr}^h(A_1)   m \rangle$
$C_S^{ss}$	$\langle n_a   O_{ss}(A_1)   n_a \rangle$	$\langle m'   H_{ss}(A_1)   m \rangle$
...	$\langle n_b   O_{ss}(A_1)   n_b \rangle$	$\langle m'   H_{ss}(A_1)   m \rangle$
$C_A^{ss}$	$\langle n_a   O_{ss}(E_a)   n_a \rangle$	$\langle m'   H_{ss}(E_a)   m \rangle$
...	$-\langle n_b   O_{ss}(E_a)   n_b \rangle$	$\langle m'   H_{ss}(E_a)   m \rangle$
...	$-\langle n_a   O_{ss}(E_b)   n_b \rangle$	$\langle m'   H_{ss}(E_b)   m \rangle$
$C_S^{ss,h}$	$\langle n_a   O_{ss}^h(A_1)   n_a \rangle$	$\langle m'   H_{ss}^h(A_1)   m \rangle$
...	$\langle n_b   O_{ss}^h(A_1)   n_b \rangle$	$\langle m'   H_{ss}^h(A_1)   m \rangle$
$C_A^{ss,h}$	$\langle n_a   O_{ss}^h(E_a)   n_a \rangle$	$\langle m'   H_{ss}^h(E_a)   m \rangle$
...	$-\langle n_b   O_{ss}^h(E_a)   n_b \rangle$	$\langle m'   H_{ss}^h(E_a)   m \rangle$
...	$-\langle n_a   O_{ss}^h(E_b)   n_b \rangle$	$\langle m'   H_{ss}^h(E_b)   m \rangle$
$C_S^{st}$	$\langle n_a   O_{st}(A_1)   n_a \rangle$	$\langle m'   H_{st}(A_1)   m \rangle$
...	$\langle n_b   O_{st}(A_1)   n_b \rangle$	$\langle m'   H_{st}(A_1)   m \rangle$
$C_A^{st}$	$\langle n_a   O_{st}(E_a)   n_a \rangle$	$\langle m'   H_{st}(E_a)   m \rangle$
...	$-\langle n_b   O_{st}(E_a)   n_b \rangle$	$\langle m'   H_{st}(E_a)   m \rangle$
...	$-\langle n_a   O_{st}(E_b)   n_b \rangle$	$\langle m'   H_{st}(E_b)   m \rangle$
$C_S^{st,h}$	$\langle n_a   O_{st}^h(A_1)   n_a \rangle$	$\langle m'   H_{st}^h(A_1)   m \rangle$
...	$\langle n_b   O_{st}^h(A_1)   n_b \rangle$	$\langle m'   H_{st}^h(A_1)   m \rangle$

<sup>a</sup>Dots mean that the hyperfine coupling constant appears in one of the preceding rows.

<sup>b</sup>The hyperfine coupling constant is equal to the matrix element of a rotation-torsion operator within or between the component functions  $n_a$  and  $n_b$  of a doubly degenerate rotation-torsion level.

<sup>c</sup>The hyperfine matrix element that factors the hyperfine coupling constant is given in this column.  $|m\rangle$  and  $|m'\rangle$  are shorthand notations for  $|J, \mu, I, F\rangle$  and  $|J, \mu', I', F\rangle$ , respectively, where  $\mu, \mu' = E_a$  or  $E_b$ .

TABLE IV. Reduction coefficients<sup>a</sup> for the spin-rotation and spin-torsion couplings.

$\Gamma^b$	$\mu'$	$\mu$	$I'$	$I$	$C_{sr}^\Gamma(\mu', \mu, I', I)$	$C_{sr}^{\Gamma,h}(\mu', \mu, I', I)$
$A_1$	$A_1$	$A_1$	2	2	$+\sqrt{45/4}$	$+\sqrt{5/4}$
	$A_1$	$A_1$	2	1	$-\sqrt{5/4}$	$+\sqrt{5/4}$
	$A_1$	$A_1$	1	1	$-5/2$	$+1/2$
	$E_a$	$E_a$	1	1	$-1$	$-1$
	$E_a$	$E_a$	1	0	$+\sqrt{1/2}$	$-\sqrt{1/2}$
	$E_b$	$E_b$	1	1	$-1$	$-1$
	$E_b$	$E_b$	1	0	$+\sqrt{1/2}$	$-\sqrt{1/2}$
$E_a$	$E_a$	$E_a$	1	1	$+1$	0
	$E_a$	$E_a$	1	0	$-\sqrt{1/2}$	0
	$E_b$	$E_b$	1	1	$-1$	0
	$E_b$	$E_b$	1	0	$+\sqrt{1/2}$	0
	$E_b$	$E_b$	1	0	$+\sqrt{1/2}$	0
$E_b$	$E_a$	$E_b$	1	1	$-1$	0
	$E_a$	$E_b$	1	0	$+\sqrt{1/2}$	0
	$E_b$	$E_a$	1	1	$-1$	0
	$E_b$	$E_a$	1	0	$+\sqrt{1/2}$	0

<sup>a</sup>Reduction coefficients depend on the symmetry species,  $\mu'$  and  $\mu$ , and on the total nuclear spin,  $I'$  and  $I$ , characterizing the nuclear spin wavefunctions in Eqs. (13). A superscripted  $h$  indicates reduction coefficients corresponding to a hyperfine operator involving the contribution of the hydroxyl group hydrogen atom.

<sup>b</sup> $\Gamma$  is the symmetry species characterizing the hyperfine operators. For hyperfine operators including the contribution from the hydroxyl group hydrogen atom,  $\Gamma$  can only be  $A_1$ .

two component functions  $n_a$  and  $n_b$ . The hyperfine coupling constants and corresponding hyperfine matrix elements are reported in Table III. Equation (14) leads to 24 terms but to only 10 hyperfine coupling constants as rotation-torsion matrix elements can be related to each other using symmetry considerations. Also, only 10 hyperfine operators arise.

The hyperfine matrix elements in Eq. (15) and in Tables II and III can be calculated using Eqs. (17) and (18) of Tudorie *et al.*<sup>12</sup> where the  $(-1)^{I_1}$  factor should be ignored. For the hyperfine operators  $H_{sr}(\Gamma)$ , with  $\Gamma = A_1, E_a$ , and  $E_b$ , Eq. (17) of this reference should be used recomputing the reduced matrix element with the nuclear spin wavefunctions in Eqs. (13). This also applies for the hyperfine operators  $H_{sr}^h(A_1)$ , except that the recomputed reduction coefficients will be denoted  $C_{sr}^{A_1,h}(\mu', \mu, I', I)$ . In the case of the hyperfine operators  $H_{ss}(\Gamma)$  and  $H_{ss}^h(\Gamma)$ , with  $\Gamma = A_1, E_a$ , and  $E_b$ , Eq. (18) of Tudorie *et al.*<sup>12</sup>

should be used. Reduction coefficients should also be recomputed and those corresponding to hyperfine operators involving the contribution from the hydroxyl group hydrogen atom will be denoted  $C_{ss}^{\Gamma,h}(\mu', \mu, I', I)$ . The reduction coefficients are reported in Table IV for hyperfine operators involved in the spin-rotation and spin-torsion couplings and in Table V for hyperfine operators involved in the spin-spin coupling. Only values between symmetry species having the same degeneracy, needed in the present investigation, are listed. When using Tables IV and V, it should be kept in mind that reduction coefficients are invariant under an exchange of the total nuclear spin quantum numbers  $I'$  and  $I$ .

Using the linear combination of rotation-torsion-nuclear spin wavefunction obeying the Pauli exclusion principle given in Section 3.4 of Coudert and Lopez<sup>5</sup> and the results of the present section, it can be shown that hyperfine energies of a nondegenerate rotation-torsion level  $n$  should be obtained diagonalizing a matrix  $M$  setup using Table II and the reduction coefficients in Tables IV and V with  $\mu' = \mu = A_1$ . For a given  $F$ -value, matrix elements of  $M$  between two values  $I'$  and  $I$  of the total nuclear spin angular momentum are

$$\begin{aligned}
M_{I',I} = & (-1)^{J+F} \begin{Bmatrix} F & I' & J \\ 1 & J & I \end{Bmatrix} \langle J \| J^{(1)} \| J \rangle \\
& \times [(C_S^{sr} + C_S^{st}) C_{sr}^{A_1}(A_1, A_1, I', I) \\
& + (C_S^{sr,h} + C_S^{st,h}) C_{sr}^{A_1,h}(A_1, A_1, I', I)] \\
& + (-1)^{J+F} \begin{Bmatrix} F & I' & J \\ 2 & J & I \end{Bmatrix} \langle J \| J^{(2)} \| J \rangle \\
& \times [C_S^{ss} C_{ss}^{A_1}(A_1, A_1, I', I) \\
& + C_S^{ss,h} C_{ss}^{A_1,h}(A_1, A_1, I', I)], \quad (16)
\end{aligned}$$

with  $1 \leq I', I \leq 2$ . For a doubly degenerate rotation-torsion level, depending on the rotation-torsion nuclear spin wavefunction chosen,<sup>1,5</sup> hyperfine energies levels should be obtained diagonalizing two matrices  $M^+$  and  $M^-$  to be setup using Tables III and the reduction coefficients in Tables IV and V with  $\mu', \mu = E_a$  or  $E_b$ . For a given  $F$ -value, matrix elements of  $M^\pm$  between two values  $I'$  and  $I$  of the total nuclear spin angular momentum are

$$\begin{aligned}
M_{I',I}^\pm = & (-1)^{J+F} \begin{Bmatrix} F & I' & J \\ 1 & J & I \end{Bmatrix} \langle J \| J^{(1)} \| J \rangle \{ (C_S^{sr} + C_S^{st}) [C_{sr}^{A_1}(E_a, E_a, I', I) + C_{sr}^{A_1}(E_b, E_b, I', I)] \\
& + (C_S^{sr,h} + C_S^{st,h}) [C_{sr}^{A_1,h}(E_a, E_a, I', I) + C_{sr}^{A_1,h}(E_b, E_b, I', I)] \pm (C_A^{sr} + C_A^{st}) [C_{sr}^{E_a}(E_a, E_a, I', I) \\
& - C_{sr}^{E_a}(E_b, E_b, I', I) - 2C_{sr}^{E_b}(E_a, E_b, I', I)] \} / 2 + (-1)^{J+F} \begin{Bmatrix} F & I' & J \\ 2 & J & I \end{Bmatrix} \langle J \| J^{(2)} \| J \rangle \{ C_S^{ss,h} [C_{ss}^{A_1,h}(E_a, E_a, I', I) \\
& + C_{ss}^{A_1,h}(E_b, E_b, I', I)] \pm C_A^{ss,h} [C_{ss}^{E_a,h}(E_a, E_a, I', I) - C_{ss}^{E_a,h}(E_b, E_b, I', I) - 2C_{ss}^{E_b,h}(E_a, E_b, I', I)] \} / 2, \quad (17)
\end{aligned}$$

with  $0 \leq I', I \leq 1$ . In all cases, the matrices to be diagonalized are at most  $2 \times 2$ .

TABLE V. Reduction coefficients<sup>a</sup> for spin-spin coupling.

$\Gamma^b$	$\mu'$	$\mu$	$I'$	$I$	$C_{ss}^{\Gamma}(\mu', \mu, I', I)$	$C_{ss}^{\Gamma, h}(\mu', \mu, I', I)$
$A_1$	$A_1$	$A_1$	2	2	$+\sqrt{105/4}$	$+\sqrt{105/4}$
	$A_1$	$A_1$	2	1	$-\sqrt{45/4}$	$+\sqrt{45/4}$
	$A_1$	$A_1$	1	1	$-\sqrt{45/4}$	$+\sqrt{5/4}$
	$E_a$	$E_a$	1	1	0	$-\sqrt{5}$
	$E_b$	$E_b$	1	1	0	$-\sqrt{5}$
$E_a$	$E_a$	$E_a$	1	1	0	$+\sqrt{5}$
	$E_b$	$E_b$	1	1	0	$-\sqrt{5}$
$E_b$	$E_a$	$E_b$	1	1	0	$-\sqrt{5}$
	$E_b$	$E_a$	1	1	0	$-\sqrt{5}$

<sup>a</sup>Reduction coefficients depend on the symmetry species,  $\mu'$  and  $\mu$ , and on the total nuclear spin,  $I'$  and  $I$ , characterizing the nuclear spin wavefunctions in Eqs. (13). A superscripted  $h$  indicates reduction coefficients corresponding to a hyperfine operator involving the contribution of the hydroxyl group hydrogen atom.

<sup>b</sup> $\Gamma$  is the symmetry species characterizing the hyperfine operators.

#### IV. FITTING HAMILTONIAN

A fitting Hamiltonian is build expressing the symmetry adapted rotation-torsion operators introduced in Section III B with expansions written in terms of sine and cosine functions depending on the angle of internal rotation. The constants involved in these expansions are the parameters which will be varied in the analysis described in Section V. These constants are numerically evaluated in this section using *ab initio* calculations and the structure of the molecule which provides us with an initial value for the parameters considered in the analysis. These numerical values also allow to deduce Hyperfine coupling constants and to draw predicted hyperfine patterns. The symmetry group<sup>20</sup> used in this section is  $G_6$  like in most parts of Sec. III.

##### A. Fitting parameters

As shown in Section III B, there arise 4 symmetry adapted rotation-torsion operators for the spin-rotation coupling which are written as<sup>25</sup>

$$O_{sr}^l(\Gamma) = \sum_{\beta\gamma} C_{\beta\gamma}^{\Gamma, l}(\alpha) \frac{J_{\beta} J_{\gamma}}{J(J+1)}, \quad (18)$$

where  $\beta, \gamma$  run over molecule-fixed coordinates  $x, y, z$ ; the superscripted  $l$  is either blank or  $h$ ;  $\Gamma = A_1, E_a,$  and  $E_b$ ; and  $C_{\beta\gamma}^{\Gamma, l}(\alpha)$  are  $\alpha$ -dependent functions. These functions will be expanded using  $\cos p\alpha$  and  $\sin p\alpha$  functions up to  $p = 3$ . Symmetry considerations show that for  $\beta\gamma = xx, yy, zz,$  and  $xz,$

$$\begin{cases} C_{\beta\gamma}^{A_1, l}(\alpha) = c_{\beta\gamma}^{0, l} + c_{\beta\gamma}^{3, l} \cos 3\alpha, \\ C_{\beta\gamma}^{E_a, l}(\alpha) = c_{\beta\gamma}^{1, l} \cos \alpha + c_{\beta\gamma}^{2, l} \cos 2\alpha, \\ C_{\beta\gamma}^{E_b, l}(\alpha) = -c_{\beta\gamma}^{1, l} \sin \alpha + c_{\beta\gamma}^{2, l} \sin 2\alpha, \end{cases} \quad (19)$$

and for  $\beta\gamma = xy$  and  $yz,$

$$\begin{cases} C_{\beta\gamma}^{A_1, l}(\alpha) = c_{\beta\gamma}^{3, l} \sin 3\alpha, \\ C_{\beta\gamma}^{E_a, l}(\alpha) = c_{\beta\gamma}^{1, l} \sin \alpha + c_{\beta\gamma}^{2, l} \sin 2\alpha, \\ C_{\beta\gamma}^{E_b, l}(\alpha) = c_{\beta\gamma}^{1, l} \cos \alpha - c_{\beta\gamma}^{2, l} \cos 2\alpha. \end{cases} \quad (20)$$

In both equations,  $c_{\beta\gamma}^{p, l}$ , with  $0 \leq p \leq 3$ , are constants. When using Eqs. (19) and (20), in agreement with Eq. (18), it should be kept in mind that the superscripted symmetry label on the left hand side does not necessarily correspond to the symmetry species of the term on the right hand side. For the spin-rotation coupling arising from the methyl group, Eqs. (19) and (20) lead to 22 independent  $c_{\beta\gamma}^p$  constants; for the spin-rotation coupling arising from the hydroxyl group hydrogen atom, only 10  $c_{\beta\gamma}^{p, h}$  constants arise because of the restriction  $\Gamma = A_1$ . The 6 symmetry adapted rotation-torsion operators describing the spin-spin coupling are written as<sup>25</sup>

$$O_{ss}^l(\Gamma) = \sum_{\beta\gamma} 2R_{\beta\gamma}^{\Gamma, l}(\alpha) \frac{J_{\beta} J_{\gamma}}{J(2J-1)(J+1)(2J+3)}, \quad (21)$$

where  $\beta, \gamma$  run over molecule-fixed coordinates  $x, y, z$ ;  $l$  and  $\Gamma$  are defined as for Eq. (18); and  $R_{\beta\gamma}^{\Gamma, l}(\alpha)$  are  $\alpha$ -dependent functions. These are expanded, using the same expansions as in Eqs. (19) and (20), with 44 independent constants denoted  $r_{\beta\gamma}^{p, l}$ . The 4 symmetry adapted rotation-torsion operators arising for spin-torsion coupling are written as

$$O_{st}^l(\Gamma) = \sum_{\beta} \{\rho J_z + p_{\alpha}, J_{\beta} S_{\beta}^{\Gamma, l}(\alpha)\} / [2J(J+1)], \quad (22)$$

where  $\{, \}$  is the anticommutator;  $\beta$  runs over molecule-fixed coordinates  $x, y, z$ ;  $l$  and  $\Gamma$  are defined as for Eq. (18); and  $S_{\beta}^{\Gamma, l}(\alpha)$  are  $\alpha$ -dependent functions. Using the same kind of expansion as above, it is found that for  $\beta = x$  and  $z$ , these functions can be written as

$$\begin{cases} S_{\beta}^{A_1, l}(\alpha) = s_{\beta}^{0, l} + s_{\beta}^{3, l} \cos 3\alpha, \\ S_{\beta}^{E_a, l}(\alpha) = s_{\beta}^{1, l} \cos \alpha + s_{\beta}^{2, l} \cos 2\alpha, \\ S_{\beta}^{E_b, l}(\alpha) = -s_{\beta}^{1, l} \sin \alpha + s_{\beta}^{2, l} \sin 2\alpha, \end{cases} \quad (23)$$

and for  $\beta = y,$

$$\begin{cases} S_y^{A_1, l}(\alpha) = s_y^{3, l} \sin 3\alpha, \\ S_y^{E_a, l}(\alpha) = s_y^{1, l} \sin \alpha + s_y^{2, l} \sin 2\alpha, \\ S_y^{E_b, l}(\alpha) = s_y^{1, l} \cos \alpha - s_y^{2, l} \cos 2\alpha, \end{cases} \quad (24)$$

where  $s_{\beta}^{p, l}$ , with  $0 \leq p \leq 3$ , are constants. For the spin-torsion coupling arising from the methyl group, Eqs. (23) and (24) show that 11 independent  $s_{\beta}^p$  constants arise; for the spin-torsion coupling arising from the hydroxyl group hydrogen atom, there are only 5  $s_{\beta}^{p, h}$  constants because  $\Gamma$  can only be  $A_1$ .

A total of 92 independent constants are needed to parameterize the hyperfine coupling. Although the actual number of constants is smaller than that due to relations dealt with in Sec. IV B, it is still quite large and only a small fraction of them will be refined in the analysis of the hyperfine patterns described in Section V.

##### B. Rotation-torsion operator constants

Constants involved in the spin-rotation, spin-spin, and spin-torsion operators were obtained evaluating the corresponding coupling tensor for 36 configurations with  $\alpha = 0^\circ, 10^\circ, \dots, 350^\circ$  using the atom positions from Venkateswarlu and Gordy.<sup>28</sup>

*Ab initio* calculations were carried with the ACES2 package<sup>29</sup> at the CCSD(T) level,<sup>30</sup> with basis set pVTZ,<sup>31</sup> using

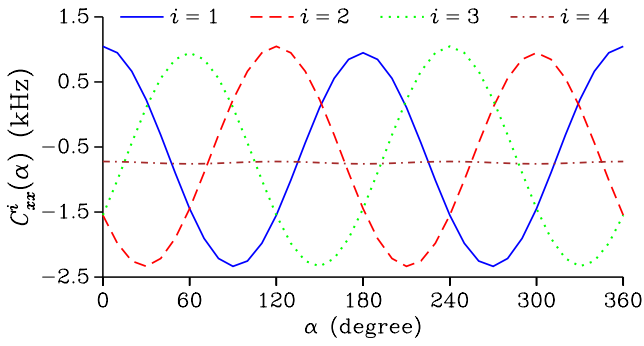


FIG. 3. The  $xx$  component of the spin-rotation coupling tensor  $\mathbf{C}^i(\alpha)$  of hydrogen atom  $i$  plotted in kHz as a function of the angle of internal rotation  $\alpha$ . Solid, dashed, dotted, and dashed-dotted lines correspond to  $i = 1, 2, 3$ , and 4, respectively.

gauge-including atomic orbitals<sup>32</sup> (GIAOs). The spin-rotation coupling tensors  $\mathbf{C}^i(\alpha)$  of the four hydrogen atoms were evaluated for the above configurations. Figure 3 shows the variations of the diagonal  $xx$  component. The symmetry adapted tensor constants were determined through a linear least-squares fitting to the *ab initio* tensor component values. Nondiagonal components were symmetrized. The root-mean-square (RMS) deviation of the fits was at most  $10^{-4}$  kHz. Constant values are given in Table VI for  $O_{sr}(A_1)$ ,  $O_{sr}(E_a)$ , and  $O_{sr}^h(A_1)$ . The largest values are for the diagonal  $zz$  component of  $O_{sr}(A_1)$  and  $O_{sr}^h(A_1)$ .

Spin-spin coupling tensors were retrieved for the same 36 configurations and for the 6 pairs of hydrogen atoms using the theoretical results in Section II A of Thaddeus *et al.*<sup>7</sup> Numerical values for the symmetry adapted tensor constants were also obtained through a linear least-squares fitting of tensor components. The RMS values were smaller than 0.1 kHz. Results are reported in Table VII for  $O_{ss}(A_1)$ ,  $O_{ss}(E_a)$ ,  $O_{ss}^h(A_1)$ , and  $O_{ss}^h(E_a)$ . For the two first operators, many constants vanish due to the fact that the structure taken in the calculation assumes a rigid methyl group with  $C_{3v}$  symmetry.<sup>28</sup> For all operators in Table VII, constants are compatible with their zero trace.

TABLE VI. Numerical values for the constants<sup>a</sup> involved in the symmetry adapted rotation-torsion operators describing spin-rotation coupling.

$O_{sr}(A_1)$		$O_{sr}(E_a)$		$O_{sr}^h(A_1)$	
$c_{xx}^0$	-0.666 29	$c_{xx}^1$	0.066 67	$c_{xx}^{0,h}$	-0.741 07
$c_{xx}^3$	-0.017 11	$c_{xx}^2$	1.665 96	$c_{xx}^{3,h}$	0.017 96
$c_{yy}^0$	-0.754 76	$c_{yy}^1$	0.009 68	$c_{yy}^{0,h}$	-2.851 60
$c_{yy}^3$	0.001 26	$c_{yy}^2$	-1.662 43	$c_{yy}^{3,h}$	-0.038 36
$c_{zz}^0$	-12.626 34	$c_{zz}^1$	-0.016 40	$c_{zz}^{0,h}$	-12.877 33
$c_{zz}^3$	0.041 09	$c_{zz}^2$	0.053 05	$c_{zz}^{3,h}$	-0.346 88
$c_{xz}^0$	0.166 21	$c_{xz}^1$	2.946 69	$c_{xz}^{0,h}$	3.655 69
$c_{xz}^3$	0.049 36	$c_{xz}^2$	-0.011 13	$c_{xz}^{3,h}$	0.024 65
$c_{xy}^3$	0.008 78	$c_{xy}^1$	-0.016 87	$c_{xy}^{3,h}$	-0.023 02
		$c_{xy}^2$	-1.664 86		
$c_{yz}^3$	-0.046 11	$c_{yz}^1$	-3.071 57	$c_{yz}^{3,h}$	-0.013 69
		$c_{yz}^2$	-0.005 82		

<sup>a</sup>Constants in kHz are defined in Eqs. (19) and (20) and obtained through the *ab initio* calculations described in Section IV B.

TABLE VII. Numerical values for the constants<sup>a</sup> involved in the symmetry adapted rotation-torsion operators describing spin-spin coupling.

$O_{ss}(A_1)$					
$r_{xx}^0$	-10.560 63	$r_{yy}^0$	-10.560 97	$r_{zz}^0$	21.121 60
$r_{xz}^0$	-0.103 44				
$O_{ss}(E_a)$		$O_{ss}^h(A_1)$		$O_{ss}^h(E_a)$	
$r_{xx}^2$	31.682 57	$r_{xx}^{0,h}$	5.147 71	$r_{xx}^{1,h}$	-6.645 90
		$r_{xx}^{3,h}$	0.239 92	$r_{xx}^{2,h}$	-0.090 66
$r_{yy}^2$	-31.682 91	$r_{yy}^{0,h}$	5.964 27	$r_{yy}^{1,h}$	-2.477 96
		$r_{yy}^{3,h}$	-0.714 69	$r_{yy}^{2,h}$	2.383 37
$r_{zz}^2$	0.000 34	$r_{zz}^{0,h}$	-11.111 98	$r_{zz}^{1,h}$	9.123 86
		$r_{zz}^{3,h}$	0.474 77	$r_{zz}^{2,h}$	-2.292 71
$r_{xz}^2$	0.103 44	$r_{xz}^{0,h}$	4.238 69	$r_{xz}^{1,h}$	5.198 86
		$r_{xz}^{3,h}$	0.485 88	$r_{xz}^{2,h}$	-2.004 58
$r_{xy}^2$	31.682 74	$r_{xy}^{3,h}$	0.454 49	$r_{xy}^{1,h}$	-2.505 57
				$r_{xy}^{2,h}$	-1.127 78
$r_{yz}^2$	0.103 44	$r_{yz}^{3,h}$	0.645 33	$r_{yz}^{1,h}$	8.451 96
				$r_{yz}^{2,h}$	-2.791 68

<sup>a</sup>Constants in kHz are defined in Eqs. (19)–(21) and obtained from the structure in Ref. 28. Values are compatible with the zero trace of the tensors.

Accounting only for the nuclear spin contribution and ignoring electronic effects,<sup>7,10</sup> spin-torsion coupling tensors were retrieved using Eqs. (14b), (16a), and (17b) of Heuvel and Dymanus<sup>10</sup> for the 4 hydrogen atoms and for the 36 above configurations. Numerical values for the symmetry adapted tensor parameters were also obtained through a linear least-squares fitting of tensor components. The RMS values were smaller than  $10^{-2}$  kHz and the results are reported in Table VIII for  $O_{st}(A_1)$ ,  $O_{st}(E_a)$ , and  $O_{st}^h(A_1)$ . Keeping in mind that the numerical values in this table may be overestimated, it should nonetheless be pointed out that the largest constants arise for the latter operator.

### C. Hyperfine coupling constants and predicted patterns

Rotation-torsion spectroscopic parameters for methanol were retrieved fitting the high resolution data reported by Xu *et al.*<sup>13</sup> up to  $J = 20$  and  $v_t = 1$  only.<sup>33</sup> These maximum values were adopted because in the fitted data set, the maximum  $J$ -

TABLE VIII. Numerical values for the constants<sup>a</sup> involved in the symmetry adapted rotation-torsion operators describing spin-torsion coupling.

$O_{st}(A_1)$		$O_{st}(E_a)$		$O_{st}^h(A_1)$	
$s_x^0$	7.748 26	$s_x^1$	-12.011 80	$s_x^{0,h}$	53.461 21
$s_x^3$	-0.148 34	$s_x^2$	0.698 76	$s_x^{3,h}$	-0.434 84
$s_y^3$	-0.064 17	$s_y^1$	-8.615 18	$s_y^{3,h}$	-0.225 73
		$s_y^2$	0.153 20		
$s_z^0$	-27.513 35	$s_z^1$	2.096 58	$s_z^{0,h}$	59.980 14
$s_z^3$	0.082 71	$s_z^2$	-0.514 33	$s_z^{3,h}$	0.185 17

<sup>a</sup>Constants in kHz are defined in Eqs. (23) and (24) and obtained from the structure in Ref. 28. Only the nuclear spin contribution is taken into account in this calculation.

TABLE IX. Numerical values for the hyperfine coupling constants<sup>a</sup> of non-degenerate levels.

Level <sup>b</sup>	$C_S^{sr}$	$C_S^{sr,h}$	$C_S^{ss}$	$C_S^{ss,h}$	$C_S^{st}$	$C_S^{st,h}$
$1_{01}A_2$	-0.71	-1.80	-4.22	2.17	0.0	0.0
$1_{11}A_2$	-6.68	-7.94	2.11	-1.04	3.31	-7.22
$1_{10}A_1$	-6.64	-6.95	2.11	-1.13	3.31	-7.22
$2_{02}A_1$	-0.71	-1.80	-1.01	0.52	0.0	0.0
$2_{12}A_1$	-2.71	-4.18	-0.50	0.27	1.11	-2.40
$2_{11}A_2$	-2.68	-3.19	-0.50	0.25	1.10	-2.40
$3_{03}A_2$	-0.71	-1.81	-0.47	0.24	0.0	0.0
$3_{13}A_2$	-1.72	-3.24	-0.35	0.19	0.55	-1.20
$3_{12}A_1$	-1.69	-2.25	-0.35	0.18	0.55	-1.20

<sup>a</sup>Constants in kHz are defined in Table II.

<sup>b</sup>Nondegenerate  $v_t = 0$  levels are labeled using  $J, K_a, K_c$ , and their symmetry species.

and  $v_t$ -values are 9 and 0, respectively. These spectroscopic parameters were used to compute rotation-torsion wavefunctions fulfilling the symmetry requirements of Coudert and Lopez,<sup>5</sup> to evaluate the matrix elements of the hyperfine coupling rotation-torsion operators introduced in Section III A, and to obtain numerical values for the hyperfine coupling constants defined in Section III C. Table IX gives the results for nondegenerate  $v_t = 0$  levels up to  $J = 3$  and  $K_a = 1$ . It can be seen that for these levels, the hyperfine spin-torsion coupling constants  $C_S^{st}$  and  $C_S^{st,h}$  exhibit a fast variation with  $K_a$ . They are zero for  $K_a = 0$  and have the same value for both members of the  $K_a = 1$  asymmetry doublet. The numerical values in Table IX can be compared with those of Heuvel and Dymanus<sup>9</sup> accounting for the different definitions used by these authors. As can be gathered from Section 3 of their paper,  $D_{J\gamma}^{(1)} = 3J(2J - 1)C_S^{ss}$  and  $D_{J\gamma}^{(2)} = 3J(2J - 1)C_S^{ss,h}$  for spin-spin coupling and  $C_{J\gamma}^{(1)} = 3C_S^{sr}$  and  $C_{J\gamma}^{(2)} = C_S^{sr,h}$  for spin-rotation coupling. Using these relations, a good agreement is obtained with Table II of these authors for the fitted and calculated spin-spin coupling constants. For the spin-rotation constants, the agreement is not as satisfactory.

For doubly degenerate rotation-torsion levels  $J_k$ , Fig. 4 shows the variations of the spin-torsion coupling constant  $C_S^{st}$  as a function of  $k$  for  $J = 6$  and  $v_t = 0$  and 1. This figure emphasizes that the coupling constant is zero for  $k = 0$  and that its variations are not smooth. The absolute value of

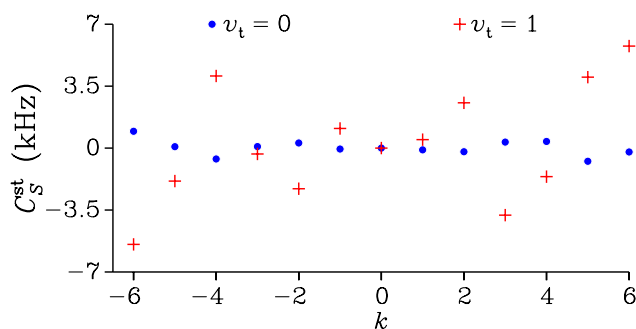


FIG. 4. The variations of the spin-torsion hyperfine coupling constant  $C_S^{st}$  for doubly degenerate rotation-torsion  $J_k$  levels with  $J = 6$  and  $-6 \leq k \leq 6$ . Full circles and crosses correspond to  $v_t = 0$  and 1, respectively.

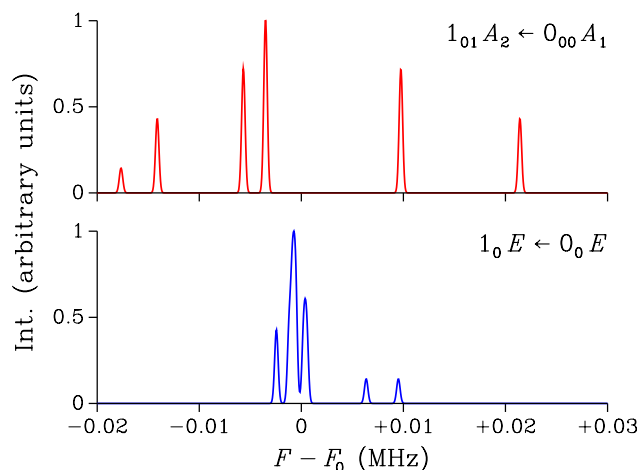


FIG. 5. The upper and lower panels show calculated hyperfine pattern for the  $1_{01}A_2 \leftarrow 0_{00}A_1$  transition at 48 372 MHz and the  $1_0E \leftarrow 0_0E$  transition at 48 376 MHz, respectively. Both patterns were plotted as a function of the difference in MHz between the frequency  $F$  and the center frequency  $F_0$  of the rotation-torsion transitions. A Gaussian line profile with a half width at half height of 0.2 kHz is used.

the coupling constant increases when going from  $v_t = 0$  to  $v_t = 1$ .

Predicted hyperfine patterns were computed using the results of Secs. IV A and IV B and evaluating the intensity of hyperfine components with Eqs. (29)–(31) of Thaddeus *et al.*<sup>7</sup> Depending on the rotation-torsion levels involved, hyperfine patterns consist of up to 38 components and the sum of all hyperfine intensities being always equal to 8. Figure 5 shows calculated hyperfine patterns of two  $J = 1 \leftarrow 0$  parallel transitions with  $v_t = 0$ . The transition involving nondegenerate rotation-torsion levels displays larger splittings that are mainly due to the spin-spin coupling. This hyperfine pattern compares very well with the observed one in Fig. 2(a) of Heuvel and Dymanus.<sup>9</sup>

## V. ANALYSIS

In the line position analysis, hyperfine energies were computed using Section III and a least-squares-fit procedure was carried out. The parameters of this procedure include the center frequency  $F_0$  of the fitted rotation-torsion transitions and the rotation-torsion operator constants introduced in Section IV. For parameters involved in the spin-rotation and spin-spin couplings, the values calculated in Section IV B were taken as initial values of the least-squares-fit procedure; for parameters involved in the spin-torsion coupling, the initial values were set to zero.

The 12 hyperfine patterns considered in the analysis are listed in Table I. The only rotation-torsion transition displaying a fully resolved hyperfine pattern is the  $1_{01}A_2 \leftarrow 0_{00}A_1$  line at 48 372 MHz and all its hyperfine components were included in the data set. As indicated by Table I, for the remaining transitions, the hyperfine patterns are partially resolved displaying either a singlet or a doublet structure. In the latter case, in agreement with Heuvel and Dymanus,<sup>9</sup> it was assumed that this is because spin-rotation coupling from the hydroxyl group hydrogen atom is dominant. For such transitions, the 8

TABLE X. Parameters determined in the analysis.

Transition <sup>a</sup>	$N^b$	Uncertainty <sup>c</sup>	$F_0^d$
$2_{1,1}A_2 \leftarrow 2_{1,2}A_1$	6	1.0	2502.7783(4)
$3_{1,2}A_1 \leftarrow 3_{1,3}A_2$	8	1.0	5005.3209(4)
$5_{1,5}A_2 \leftarrow 6_{0,6}A_1$	8	1.0	6668.5188(4)
$2_0E \leftarrow 3_{-1}E$	8	2.0	12178.6002(8)
$6_{1,5}A_2 \leftarrow 6_{1,6}A_1$	8	1.0	17513.3413(4)
$2_1E \leftarrow 3_0E$	8	4.0	19967.3914(15)
$3_2E \leftarrow 3_1E$	8	2.0	24928.6994(8)
$4_2E \leftarrow 4_1E$	8	2.0	24933.4693(8)
$2_2E \leftarrow 2_1E$	8	4.0	24934.3801(16)
$5_2E \leftarrow 5_1E$	8	2.0	24959.0781(8)
$6_2E \leftarrow 6_1E$	8	2.0	25018.1215(8)
$1_{0,1}A_2 \leftarrow 0_{0,0}A_1$	10	1.0	48372.4555(3)
Constants <sup>e</sup>			
$c_{zz}^0 - 1.766(910)$		$c_z^{0,h} - 28.535(1055)$	
		$s_z^{0,h} 69.290(12625)$	

<sup>a</sup>The assignment of the rotation-torsion transitions included in the analysis is given. All transitions are within the ground  $v_t = 0$  torsional level.

<sup>b</sup>The number of fitted hyperfine components is given.

<sup>c</sup>The experimental uncertainty used in the fit is given in kHz.

<sup>d</sup>The center frequency of the hyperfine pattern is given in MHz. Its uncertainty is given in parentheses in  $10^{-1}$  kHz.

<sup>e</sup>The rotation-torsion operator constants are defined in Section IV. Values are given in kHz and uncertainties are given in parentheses in  $10^{-3}$  kHz.

strongest hyperfine components were introduced in the data set and assigned to either member of the doublet examining the value of the derivative of the hyperfine energy with respect to  $C_S^{sr,h}$ , which is the constant describing spin-rotation coupling from the hydroxyl group hydrogen atom. For the three transitions displaying a singlet structure, the 8 strongest hyperfine components were fitted to the frequency of the singlet. This assignment process was carried out for each cycle of the least-squares-fit procedure. For the low  $J$ -value singlet transition at 2502 MHz, only the 6 strongest hyperfine components were selected. For each transition, Table X lists the number of fitted hyperfine components and the experimental uncertainty used. A large value was used for hyperfine patterns displaying broad components like that of the  $2_2E \leftarrow 2_1E$  rotation-torsion transition at 24934 MHz.

Two analyses were performed. In the first one, in addition to the 12 center frequencies, the two spin-rotation coupling constants  $c_{zz}^0$  and  $c_z^{0,h}$  were varied since, as confirmed by Table VI, they are the largest constants for this coupling and are probably calculated with the least accuracy due to the complicated nature of the magnetic spin-rotation coupling. In the first analysis, the unitless standard deviation of the fit was 1.2. In the second analysis, in addition to the same constants, the spin-torsion coupling constant  $s_z^{0,h}$  was varied because, as indicated by Table VIII, it is among those having the largest values. In this second analysis, the unitless standard deviation of the fit was only 1.1. In both analyses, a fast convergence of the least-squares-fit procedure indicates that the fitted parameters were well determined. Table X lists the value of the 15 parameters obtained in the second analysis. For spin-rotation coupling constants, these values should be compared to those in Table VI. For  $c_{zz}^0$  and  $c_z^{0,h}$ , large decrease and increase can be seen, respectively. For the spin-torsion coupling constant

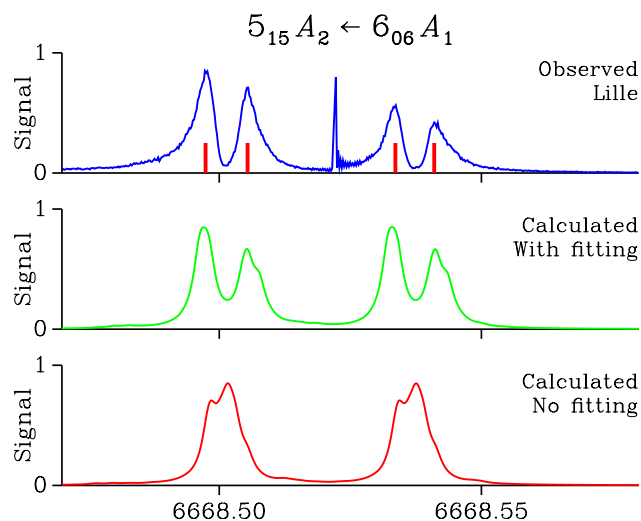


FIG. 6. Comparison between observed and calculated hyperfine patterns for the  $5_{16}A_2 \leftarrow 6_{06}A_1$  rotation-torsion transition. The upper panel displays the observed hyperfine pattern recorded with the experimental setup in Lille; the lower panel shows the calculated hyperfine pattern obtained without fitting hyperfine coupling parameters; and the middle panel shows the calculated hyperfine pattern corresponding to the second analysis. Both calculated patterns were plotted using a Doppler splitting of 17.9 kHz and a Lorentzian line profile with a half width at half height of 1.5 kHz. All three patterns display a doublet structure because spin-rotation coupling from the hydroxyl group hydrogen atom is dominant.

$s_z^{0,h}$ , there is no theoretical estimate, but its value was expected to be smaller than that in Table VIII which is believed to be overestimated. The  $c_{zz}^0$ ,  $c_z^{0,h}$ , and  $s_z^{0,h}$  coupling constants, in addition to being among the ones having the largest predicted values, are also those leading to a physically satisfactory fit. Fitting other coupling constants barely altered the residuals or led to unsatisfactory fits with too large values of the coupling constants.

Figures 6 and 7 show comparisons between observed and calculated hyperfine patterns. For each figure, there are

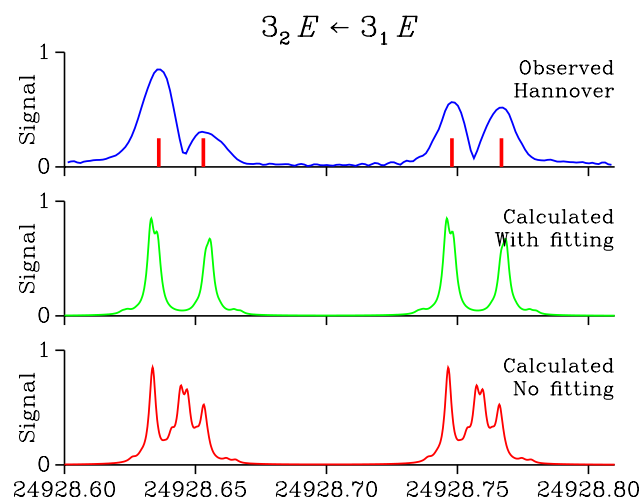


FIG. 7. The same results as in Fig. 6 for the  $3_2E \leftarrow 3_1E$  rotation-torsion transition recorded using the experimental setup in Hannover. Both calculated patterns were plotted using a Doppler splitting of 56.4 kHz and a Lorentzian line profile with a half width at half height of 1.5 kHz. The calculated hyperfine pattern in the lower panel displays a quartet structure with large and small splittings due to spin-rotation coupling from the hydroxyl group hydrogen atom and from the methyl group, respectively.

two calculated hyperfine patterns. The first one was obtained without adjusting hyperfine coupling parameters; the second one corresponds to the second analysis. The hyperfine pattern in Fig. 6 is a doublet dominated by spin-rotation coupling effects from the hydroxyl group hydrogen atom. This figure shows that before adjusting the hyperfine coupling parameters, the calculated splitting was too small. Adjusting these parameters leads to a larger splitting and this is consistent with the large increase of  $c_{zz}^{0,h}$ . The hyperfine pattern in Fig. 7 is a quartet with a large splitting also due to spin-rotation coupling effects from the hydroxyl group hydrogen atom and a small splitting due to spin-rotation coupling effects from the methyl group. When adjusting the hyperfine coupling parameters, the large splitting increases while the smaller one collapses leading to a doublet structure. Just like in Fig. 6, this increase is consistent with the increase of  $c_{zz}^{0,h}$ . The disappearance of the smaller splitting is, however, consistent with the large decrease of  $c_{zz}^0$ .

A figure showing comparisons between observed and calculated hyperfine patterns for the 19 rotation-torsion listed in Table I is available in the supplementary material.<sup>19</sup> It reveals that there is a good agreement except for the  $4_{32} A_1 \leftarrow 5_{23} A_2$  and the  $9_{-1} E \leftarrow 8_{-2} E$  transitions, not included in the analysis as already stressed in Section II, and the  $2_2 E \leftarrow 2_1 E$  transitions, included in the analysis. For the latter, the calculated doublet structure does not match the observed singlet structure. The large width of the observed singlet line suggests, however, that the experimental hyperfine pattern probably is an unresolved doublet. For the  $1_{0,1} A_2 \leftarrow 0_{0,0} A_1$  transition, there is very little change after the fitting. This stems from the nature of its hyperfine pattern, dominated by spin-spin coupling, and from the fact that no parameters corresponding to this coupling are varied in the analysis. The numerical values in Table IX are also consistent with the nature of this hyperfine pattern.

## VI. DISCUSSION

Experimental hyperfine patterns recorded in this work and in a previous experimental investigation<sup>9</sup> for the non-rigid methanol molecule are analyzed using an approach accounting for the interaction between the magnetic hyperfine coupling and the large amplitude motion. The latter leads to averaging effects as the torsional motion exchanges the three protons of the methyl group giving rise to hyperfine coupling. As emphasized in Section IV A, the fitting Hamiltonian derived using symmetry considerations to compute the hyperfine energy depends on a very large number of parameters because up to four atoms give rise to hyperfine coupling and the variation of the coupling with the angle of internal rotation must be accounted for.<sup>5,12</sup>

In the hyperfine structure of methanol, evidencing the effects of the so called spin-torsion coupling<sup>9-11</sup> is an important issue. This hyperfine coupling is due to the additional magnetic field caused by the internal rotation of the methyl group which interacts with the nuclear spin of the four hydrogen atoms. The spin-torsion coupling is taken into account in the present investigation [Eq. (5)] but the exact magnitude of the corresponding coupling constants is difficult to obtain. A tentative determination of these is carried out in Section IV C accounting only for the nuclear contribution and ignoring the electronic

contribution. The resulting constants, given in Table VIII, are probably overestimated due to this approximation. As stressed by Eqs. (6) and (11), the spin-torsion coupling leads to the same hyperfine operators than the spin-rotation coupling. More precisely, the spin-torsion coupling gives rise to an additional contribution to the spin-rotation coupling constants. Indeed, the hyperfine matrix elements in Eqs. (16) and (17) depend only on the sum  $C^{sr} + C^{st}$  of the spin-rotation and spin-torsion hyperfine coupling constants. The effects of spin-torsion are strongly dependent on the unsigned quantum number  $K_a$  for nondegenerate levels and on the signed quantum number  $k$  for doubly degenerate levels. This can be seen in Fig. 4 for the latter type of levels. This figure also shows that these effects increase with  $v_r$ .

In the line position analysis of the experimental hyperfine patterns, 12 rotation-torsion transitions were considered including 5 transitions involving nondegenerate levels and 7 involving doubly degenerate levels. Only one observed hyperfine pattern was fully resolved, the remaining ones displaying either a singlet or a doublet structure. This could be qualitatively understood assuming that the spin-rotation coupling effects from the hydrogen atom of the hydroxyl group were dominant. Before the fitting, as emphasized by Figs. 6 and 7 and by one of the figures available in the supplementary material,<sup>19</sup> the agreement between observed and calculated hyperfine patterns was somewhat satisfactory for transitions involving nondegenerate levels, but not for those involving doubly degenerate levels. Adjusting two hyperfine coupling parameters corresponding to spin-rotation having the largest calculated values in Section IV B allowed us to reproduce the doublet structure observed in several cases. The results of the line position analysis were further improved when spin-torsion effects were accounted for allowing us to carry out the first determination of one of the corresponding parameters. This fitted value, listed in Table X, is believed to be too large as it exceeds its estimated value retrieved in Section IV B. The comparison between observed and calculated hyperfine patterns is satisfactory except for three rotation-torsion transitions out the 19 available presented in Section II. Although the determination of the spin-torsion coupling constant should be taken with care, this work follows that of Heuvel and Dymanus<sup>9,10</sup> and presents the next step in the investigation of the hyperfine structure of the astrophysically relevant methanol molecule.<sup>6</sup>

## ACKNOWLEDGMENTS

The authors are very indebted to Vadim Ilyushin for providing them with part of the high resolution experimental data available for methanol.

<sup>1</sup>A. A. Wolf, Q. Williams, and T. L. Weatherly, *J. Chem. Phys.* **47**, 5101 (1967).

<sup>2</sup>L. H. Coudert, J. T. Hougen, and R. D. Suenram, *J. Mol. Spectrosc.* **135**, 314 (1989).

<sup>3</sup>R. L. Bhattacharjee, J. S. Muentner, and L. H. Coudert, *J. Chem. Phys.* **97**, 8850 (1992).

<sup>4</sup>W. Stahl and L. H. Coudert, *J. Mol. Spectrosc.* **157**, 161 (1993).

<sup>5</sup>L. H. Coudert and J. C. López, *J. Mol. Spectrosc.* **239**, 135 (2006).

<sup>6</sup>M. G. Kozlov and S. A. Levshakov, *Ann. Phys.* **525**, 452 (2013).

<sup>7</sup>P. Thaddeus, L. C. Krisher, and J. H. N. Loubser, *J. Chem. Phys.* **40**, 257 (1964).

- <sup>8</sup>R. M. Garvey, F. C. De Lucia, and J. W. Cederberg, *Mol. Phys.* **31**, 265 (1976).
- <sup>9</sup>J. E. M. Heuvel and A. Dymanus, *J. Mol. Spectrosc.* **45**, 282 (1973).
- <sup>10</sup>J. E. M. Heuvel and A. Dymanus, *J. Mol. Spectrosc.* **47**, 363 (1973).
- <sup>11</sup>J. T. Hougen, W. L. Meerts, and I. Ozier, *J. Mol. Spectrosc.* **146**, 8 (1991).
- <sup>12</sup>M. Tudorie, L. H. Coudert, T. R. Huet, D. Jegouso, and G. Sedes, *J. Chem. Phys.* **134**, 074314 (2011).
- <sup>13</sup>L.-H. Xu, J. Fisher, R. M. Lees, H. Y. Shi, J. T. Hougen, J. C. Pearson, B. J. Drouin, G. A. Blake, and R. Braakman, *J. Mol. Spectrosc.* **251**, 305 (2008).
- <sup>14</sup>J.-U. Grabow and W. Stahl, *Z. Naturforsch.* **45a**, 1043 (1990).
- <sup>15</sup>J.-U. Grabow, W. Stahl, and H. Dreizler, *Rev. Sci. Instrum.* **67**, 4072 (1996).
- <sup>16</sup>J.-U. Grabow, "Chemische bindung und interne dynamik in großen isolierten molekülen: Rotationsspektroskopische untersuchung," in *Habilitationsschrift* (Hannover, 2004).
- <sup>17</sup>L. Margulès, L. H. Coudert, H. Møllendal, J.-C. Guillemin, T. R. Huet, and R. Janečková, *J. Mol. Spectrosc.* **254**, 55 (2009).
- <sup>18</sup>L. Margulès, T. R. Huet, J. Demaison, M. Carvajal, I. Kleiner, H. Møllendal, B. Tercero, N. Marcelino, and J. Cernicharo, *Astrophys. J.* **714**, 1120 (2010).
- <sup>19</sup>See supplementary material at <http://dx.doi.org/10.1063/1.4926942> for two PDF files showing observed hyperfine patterns for the 19 rotation-torsion transitions considered in this work and comparisons between observed and calculated hyperfine patterns for the same transitions.
- <sup>20</sup>J. T. Hougen, I. Kleiner, and M. Godefroid, *J. Mol. Spectrosc.* **163**, 559 (1994).
- <sup>21</sup>B. Kirtman, *J. Chem. Phys.* **37**, 2516 (1962).
- <sup>22</sup>R. M. Lees and J. G. Baker, *J. Chem. Phys.* **48**, 5299 (1968).
- <sup>23</sup>E. Herbst, J. K. Messer, F. C. De Lucia, and P. Helminger, *J. Mol. Spectrosc.* **108**, 42 (1984).
- <sup>24</sup>J. T. Hougen, *J. Chem. Phys.* **57**, 4207 (1972).
- <sup>25</sup>L. H. Coudert, W. Caminati, M. Schnell, and J.-U. Grabow, *J. Mol. Spectrosc.* **242**, 118 (2007).
- <sup>26</sup>R. Bersohn, "Hyperfine structure in molecules, calculation of quadrupole fine structure in molecular rotation spectra," Ph.D. thesis, Harvard University, 1949.
- <sup>27</sup>K. K. Svidzinskii, "Theory of the hyperfine structure in the rotational spectra of molecules," in *Soviet Maser Research*, edited by D. V. Skobel'tsyn (Consultants Bureau, New York, 1964) [Proceedings of the P. N. Lebedev Physics Institute XXI (Consultants Bureau, 1963), p. 88].
- <sup>28</sup>P. Venkateswarlu and W. Gordy, *J. Chem. Phys.* **23**, 1200 (1955).
- <sup>29</sup>ACES2, a quantum chemical program package written by J. F. Stanton, J. Gauss, J. D. Watts, P. G. Szalay, and R. J. Bartlett with contribution from A. A. Auer, D. B. Bernholdt, O. Christiansen, M. E. Harding, M. Heckert, O. Heun, C. Huber, D. Jonsson, J. Jusélius, W. J. Lauderdale, T. Metzroth, K. Ruud, and the integral packages MOLECULE (J. Almlöf and P. R. Taylor), Props (P. R. Taylor), and ABACUS (T. Helgaker, H. J. Aa. Jensen, P. Jørgensen, and J. Olsen). See also J. F. Stanton, J. Gauss, J. D. Watts, W. J. Lauderdale, and R. J. Bartlett, *International Journal of Quantum Chemistry Symposium* (Wiley, 1992), Vol. 26, p. 879, as well as (<http://www.aces2.de>) for the current version.
- <sup>30</sup>K. Raghavachari, G. W. Trucks, J. A. Pople, and M. Head-Gordon, *Chem. Phys. Lett.* **157**, 479 (1989).
- <sup>31</sup>T. H. Dunning, *J. Chem. Phys.* **90**, 1007 (1989).
- <sup>32</sup>J. Gauss and J. F. Stanton, *J. Chem. Phys.* **104**, 2574 (1996).
- <sup>33</sup>V. Ilyushin, private communication (2014).